The Astrophysical Journal Letters, 943:L3 (7pp), 2023 January 20 https://doi.org/10.3847/2041-8213/acaefa

Photons' Scattering in Relativistic Plasma with Velocity Shear: Generation of High Energy Power-law Spectra

Mukesh K. Vyas and Asaf Pe'er
Bar Ilan University, Ramat Gan, 5290002, Israel; mukeshkvys@gmail.com
Received 2022 August 15; revised 2022 December 26; accepted 2022 December 26; published 2023 January 20

Abstract

A high energy power law is a common feature in the spectra of many astrophysical objects. We show that the photons in an unmagnetized relativistic plasma composed of electrons and protons with a variable Lorentz factor (or a velocity shear) go through repeated scattering with electrons to gain energy. The escaped population of photons naturally produces a power-law-shaped spectrum making it a photon's analog to the conventional Fermi acceleration mechanism for charged particles. Thus, this mechanism provides a natural alternative to current explanations of high energy power-law spectra via synchrotron or thermal Comptonization. The model is applicable to any relativistic plasma beam with an arbitrary Lorentz factor profile. We implement the theory to the gamma-ray burst prompt phase and show that the obtained range of the photon indices is compatible with the observed values and the results of Monte Carlo simulations that we carry out independently. Therefore, the observed high energy spectral indices provide a unique indicator of the jet structure.

Unified Astronomy Thesaurus concepts: High energy astrophysics (739); Gamma-ray bursts (629); Relativistic jets (1390); Theoretical models (2107)

1. Introduction

A power-law spectrum at high energies appears ubiquitously in several astrophysical sources like active galactic nuclei (Nandra & Pounds 1994; Reeves & Turner 2000; Page et al. 2005), and gamma-ray bursts (GRBs; Band et al. 1993; Preece et al. 1998, 2000; Barraud et al. 2003; Kaneko et al. 2006; Bošnjak et al. 2014; Pe'er 2015).

These objects are characterized by trans- or highly relativistic jets, namely having Lorentz factor $\Gamma \gg 1$. Such jets are produced by the collapse of a massive star, merger of two compact objects (in the case of GRBs; Levinson & Eichler 1993; Woosley 1993; MacFadyen & Woosley 1999; Vyas 2022), or through an accretion disk surrounding a black hole (Junor et al. 1999; Doeleman et al. 2012; Vyas et al. 2015; Vyas & Chattopadhyay 2017, 2018a; Le et al. 2018; Vyas & Chattopadhyay 2018b, 2019; Aneesha & Mandal 2020; Fukue 2021). Although the geometric shape of these jets is uncertain, numerical modeling shows some typical jet profiles where the jet's Lorentz factor is a function of its polar angle, (i.e., $\Gamma = \Gamma(\theta)$), which may be universal (Zhang et al. 2003; Lundman et al. 2013; Pe'er & Ryde 2017). This internal jet structure with a velocity shear within the plasma implies that the photons emitted deep inside the flow are scattered in regions with different velocities before escaping. As we show here, a part of the photon population gains energy, resulting in a power-law-shaped spectrum at high energies. This process draws similarity with second-order Fermi acceleration of charged particles interacting with randomly moving magnetic irregularities (Blandford & Eichler 1987). In this process, the photons gain energy from the bulk kinetic energy of the jet itself. In few studies, nonthermal high energy spectra due to shear layers of plasma is reported through numerical simulations (Reig et al. 2001, also see Kylafis et al. 2003; Lundman et al. 2013; Ito et al. 2013; Kaufman & Blaes 2016; Kaufman et al. 2017). However, the theoretical modeling of the process is not carried out and it is attempted in this Letter. This mechanism, thus, is a viable alternative to the known mechanisms that are invoked in producing the power-law spectra, such as synchrotron (Tavani 1996; Cohen et al. 1997; Schaefer et al. 1998; Frontera et al. 2000; Ryde & Pe'er 2009; Wang et al. 2009; Burgess et al. 2014; Pe'er 2015; Yu et al. 2015; Zdziarski et al. 2017) or inverse Compton from power-law accelerated electrons, or by thermal Comptonization (Vyas et al. 2021a, 2021b). Within this framework, the dependence of the emerging high energy spectral indices on the dynamical variables of the system thus provides a novel signature of the jet structural profile, $\Gamma = \Gamma(\theta)$.

2. Photon Energy Gain Due to Velocity Shear

An astrophysical jet can be pictured as a relativistic plasma beam expanding in space at angles $\theta \leqslant \theta_{\rm out}$ with the propagation axis being at $\theta = 0$. Assuming axial symmetry (where system parameters are independent of azimuthal rotation or change in ϕ), we consider a Lorentz factor profile of the plasma to be a function of the radial and angular coordinates, $\Gamma = \Gamma(r, \theta)$.

The conditions deep inside the jet, namely high density, high temperature, and strong magnetic fields (Pe'er 2015) imply a bright emission of photons at some characteristic inner radii r_0. These photons, then propagate and interact with the electrons inside the plasma until they escape. In describing the scattering process, we omit the random thermal motion of the electrons, an assumption that is valid as long as adiabatic losses dominate over possible heating mechanisms inside the jet. This assumption implies that the Lorentz factor associated with the thermal motion is small (i.e., $\gamma - 1 << 1$ or $\gamma \sim 1$). Further, to keep the system simple enough, we consider unmagnetized plasma consists of electrons and protons. As our main goal is to have a physical insight into the mechanism of photon energy

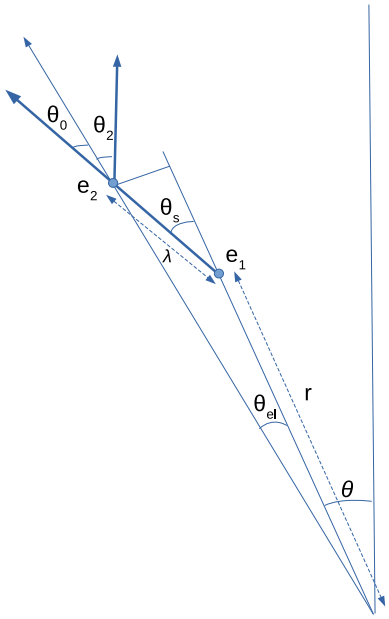

Figure 1. Geometry of scattering in lab frame in spherical coordinates r, θ, ϕ. The origin lies at the center of the star; θ is the location of a certain scattering event of the photon with electron e_1 at r radial distance; $\theta + \theta_{\rm el}$ is the angular location of the next scattering event with electron e_2; $\theta_{\rm s}$ and θ_2 are the scattering angles in the lab frame for both scattering events, respectively.

gain by shear layers of the jet, we omit all possible conditions that may lead to plasma heating. We do not refuse the possibility of hot plasma and their effects on the emergent spectra as we have explicitly dealt with such cases in our previous papers (Vyas et al. 2021a, 2021b).

As the emitted photons propagate inside the expanding jetted plasma, they gain energy (on average) by multiple scattering with the electrons. Consider a photon that undergoes a scattering with an electron having a (bulk) Lorentz factor Γ at location (r, θ), and emerges with energy ε at an angle $\theta_{\rm s}$ with respect to the direction of the electron (all quantities are measured in the lab frame; see Figure 1).

After being scattered, the photon interacts with a second electron having Lorentz factor Γ_2 at a new location, and is scattered at an angle θ_2 with emerging energy ε_2.

2.1. Average Mean Free Path and Average Scattering Angle

In order to compute the energy gain of the photons in the scattering process, we need to estimate the average mean free path at a given location as well as the average scattering angles. The mean free path λ_1 transforms from the comoving frame (λ_0) of the first electron to the lab frame as

$$\lambda_{\rm l} = \frac{\lambda_0}{\Gamma[1 - v\cos(\theta_{\rm s1})]} = \frac{\lambda_0}{\Gamma\left[1, -, v, \left[\frac{\cos(\theta'_{\rm s1}) + v}{1 + v\cos(\theta'_{\rm s1})}\right]\right]}. \quad (1)$$

Here $\theta_{\rm s1}$ is the scattering angle for the scattering event. As the photons are scattered isotropically in the comoving frame of the electron, the averaged mean free path of the photon at a given location is obtained by averaging this expression over angular region $\theta'_{\rm s1} \rightarrow 0 - \pi$

$$\lambda = \frac{\int_0^\pi \frac{\lambda_0 d\theta'_{\rm s1}}{\Gamma\left(1 - v\left[\frac{\cos(\theta'_{\rm s1}) + v}{1 + v\cos(\theta'_{\rm s1})}\right]\right)}}{\int_0^\pi d\theta'_{\rm s1}}. \quad (2)$$

It is solved to

$$\lambda = \frac{1}{\pi}\left[\frac{\lambda_0[v\sin(\theta'_{\rm s1}) + \theta'_{\rm s1}]}{\Gamma(1 - v^2)}\right]_0^\pi = \Gamma\lambda_0 = \frac{\Gamma}{n'_{\rm e}\sigma_T} \quad (3)$$

Here σ_T is the Thomson scattering cross section, $n'_{\rm e}$ is electron number density in the local comoving frame of the first electron, and v is the bulk speed of the first electron in terms of light speed.

From Equation (1), the average mean free path λ has to be associated with average scattering angle $\theta_{\rm s}$ or,

$$\lambda = \frac{\lambda_0}{\Gamma[1 - v\cos(\theta_{\rm s})]}. \quad (4)$$

From Equations (3) and (4), we have

$$\frac{\lambda_0}{\Gamma[1 - v\cos(\theta_{\rm s})]} = \Gamma\lambda_0. \quad (5)$$

Solving this equation for narrow relativistic flows with $\Gamma >> 1$ and $\theta_s << 1$, we obtain

$$\theta_{\rm s} = \frac{1}{\Gamma}. \quad (6)$$

Similarly the average scattering angle from the second electron is $\theta_2 = 1/\Gamma_2$.

2.2. Energy Gain in the Scattering Process

We consider the Thomson limit, namely that the energy of the photon before and after the second scattering, as measured in the (second) electron's rest frame, $\varepsilon'[= \Gamma_2\varepsilon(1 - v_2\cos\theta_0)]$ and $\varepsilon_2'[= \Gamma_2\varepsilon_2(1 - v_2\cos\theta_2)]$ are equal, i.e., $\varepsilon_2' = \varepsilon'$. Here v_2 is the velocity of the second electron (in units of light speed) and θ_0 is the angle between the electron's direction and the incoming photon's direction in the lab frame. Denoted by $\theta_{\rm el}$ is the angular shift of the photon location between the two scattering events in the lab frame. From the geometry, one has $\theta_0 = \theta_{\rm s} - \theta_{\rm el}$, or $\varepsilon' = \Gamma_2\varepsilon[1 - v_2\cos(\theta_{\rm s} - \theta_{\rm el})]$. The energy gain in this scattering process is therefore

$$g = \frac{\varepsilon_2}{\varepsilon} = \frac{1 - v_2\cos(\theta_{\rm s} - \theta_{\rm el})}{1 - v_2\cos(\theta_2)}. \quad (7)$$

If the local mean free path measured in the lab frame is $\lambda(r, \theta)$, then

$$\tan\theta_{\rm el} = \frac{\lambda\sin\theta_{\rm s}}{r + \lambda\cos\theta_{\rm s}} = \frac{a\theta_{\rm s}}{1 + a\cos\theta_{\rm s}} \Rightarrow \frac{\theta_{\rm el}}{\theta_{\rm s}} \approx \frac{a}{1 + a}, \quad (8)$$

where $a \equiv \lambda/r$. For a relatively small mean free path in an optically thick and dense plasma, $\lambda \ll r$,[1] one has $\Gamma_2 = \Gamma + \delta\Gamma$,

[1] The mechanism is valid for the collimated jets with narrow angles or $\theta_{\rm out} << 1$. Hence it is applied for highly relativistic jets.

namely

$$\frac{\Gamma_2}{\Gamma} = 1 + \frac{\delta\Gamma}{\Gamma} = 1 + \sum \frac{\partial \log \Gamma}{\partial x^i}\delta x^i. \quad (9)$$

Here x^i are spatial coordinates. Using these expressions in Equation (7), the gain becomes

$$g(r, \theta) \approx \frac{1}{2}\left[1 + \left[1 + \sum \frac{\partial \log \Gamma}{\partial x^i}\delta x^i\right]^2 \frac{1}{(1+a)^2}\right]. \quad (10)$$

This expression implies that the photon can gain ($g > 1$) or lose energy ($g < 1$) in a single scattering event. A sharp fractional Lorentz factor gradient followed by a large positive term $[(\partial \log \Gamma/\partial x^i)\delta x^i]$ may be sufficiently steep to overcome the adiabatic losses due to the plasma expansion (the $(1+a)^{-2}$ term). It results in a net energy gain for the photon (i.e., $g > 1$). On the other hand, the net gain due to the shear may be insufficient, in which case the energy loss due to the expansion would dominate, leading to a net energy loss, (i.e., $g < 1$).

The expression in Equation (10) can be simplified by considering axial symmetry, for which $\partial\Gamma/\partial\phi = 0$. Furthermore, for scattering at an average angle $1/\Gamma$ (Equation (6)) in the lab frame, δr is always positive, while the sign of $\delta\theta(\partial\Gamma/\partial\theta)$ depends upon the sign of $\delta\theta$. A photon can scatter away from the propagation axis ($\theta = 0$) with an average angle $\delta\theta = \theta_{\rm el}$, or it can scatter toward the axis with an average angle $\delta\theta = -\theta_{\rm el}$. Both cases have equal probabilities. If we denote the gain in these two cases by g_+ and g_-, the average gain in a single scattering at location (r, θ) is

$$g_{\rm a}(r, \theta) = \frac{g_+ + g_-}{2}.$$

The average energy gain depends both on the Lorentz factor gradient and the radial location via the parameter a. Hence, $a = \Gamma/rn'_{\rm e}\sigma_T$.

The expectation value of the photon energy gain in the plasma is evaluated by integrating the average gain over the entire region of scattering

$$\bar{g} = \frac{1}{V}\int_V g_{\rm a}(\theta, r)dV. \quad (11)$$

Here, V is the volume of total region within angular boundaries $0...\theta_{\rm out}$ and radial extend $r_0 \leqslant r \leqslant r_{\rm ph}$, where $r_{\rm ph}$ is the photospheric radius at which the photons escape to infinity. This radius depends upon the specific jet geometry.

The average probability of the photon to have a scattering without escape within the jet is the probability $P(r, \theta)$ averaged over the available volume V of scattering where the velocity shear is present, i.e.,

$$\bar{P} = \frac{1}{V}\int_V P(r, \theta)dV. \quad (12)$$

The statistical averages for the estimation of $\bar{g}$ and $\bar{P}$ are meant for a large number of photons for which all the portions of the jet are accessible. A photon can escape the scattering region through the photospheric radius or from the angular jet boundary at $\theta = \theta_{\rm b}$ (in this case, it is $\theta_{\rm out}$). In the former case, the escape probability of the photon is $\exp(-\tau_1) = \exp(-r_{\rm ph}/r)$, where τ_1 is the optical depth along the radial direction. In the latter case, the probability of escape through the angular boundary ($\theta_{\rm b}$) is calculated by estimating the optical depth along direction $\theta_{\rm s}$ (see Figure 1)

$$\tau_2 = \int_0^{s_0} \Gamma(1 - v\cos\theta_{\rm s})n'_{\rm e}\sigma ds. \quad (13)$$

Here, ds is a length element along $\theta_{\rm s}$, and the integration boundary is $s_0 = (|\theta - \theta_{\rm b}|)r/\theta_{\rm s}$. The photon entertains the minimum of these two optical depths τ_1 and τ_2 to escape the scattering region, i.e., $\tau = \min(\tau_1, \tau_2)$. Thus, the probability that the photon would escape is $P_{\rm e}(r, \theta) = \exp[-\tau(r, \theta)]$, while the probability for it to have next scattering inside the beam is $P(r, \theta) = 1 - P_e$. Using it in Equation (12) enables us to estimate $\bar{P}$.

3. Computation of Produced Spectrum

To calculate the spectrum of the escaped photons, consider that N_0 photons are homogeneously injected at $r = r_0$.[2] After scattering k times, $N = N_0\bar{P}^k$ photons are left within the scattering region. After kth scattering, the photon's average energy is $\varepsilon_{\rm k} = \varepsilon_{\rm i}\bar{g}^k$, implying

$$\frac{N}{N_0} = \left(\frac{\varepsilon_{\rm k}}{\varepsilon_{\rm i}}\right)^{\beta'}, \quad (14)$$

where $\beta' = \frac{\ln \bar{P}}{\ln \bar{g}}$. The resulting photon index of the escaped photons is

$$\beta = \beta' - 1 = \frac{\ln \bar{P}}{\ln \bar{g}} - 1. \quad (15)$$

Thus, for a given set of dynamic parameters, the high energy part of escaped photons' spectrum is characterized by a power law with photon index β. For a defined Lorentz factor profile and angular boundaries (θ_i, $\theta_{\rm out}$), radial boundaries $r_0(r, \theta, \phi)$ and $r_{\rm ph}(r, \theta, \phi)$, the photon index of the observed spectra can be evaluated directly from the equations above. The treatment is valid as long as the plasma is relativistic.

As a test case, we apply the model to the prompt phase of GRBs where, within the framework of the "collapsar" model (Levinson & Eichler 1993; Woosley 1993; MacFadyen & Woosley 1999); a jet is launched from the center of a collapsing star. Once erupted, the jet propagates along direction $\theta = 0$ above the stellar surface. As shown by Zhang et al. (2003), a relativistic GRB jet harbors an angular structure where the dependency of their Lorentz factor (Γ) on polar angle θ can be approximated by Lundman et al. (2013) and Pe'er & Ryde (2017)

$$\Gamma(\theta) = \Gamma_{\rm min} + \frac{\Gamma_0}{\sqrt{\left(\frac{\theta}{\theta_{\rm j}}\right)^{2p} + 1}}. \quad (16)$$

This profile is plotted in Figure 2. Here, $\Gamma_{\rm min}$ and Γ_0 are constants with $\Gamma_0 > \Gamma_{\rm min}$, and p is the jet profile index that shows the sharpness of the velocity gradient between shear layers of the jet. The inner region of the jet ($\theta < \theta_{\rm j}$) approaches a maximum Lorentz factor Γ_0 while the region outside $\theta_{\rm e} \sim \theta_{\rm j}\Gamma_0^{1/p}$ asymptotically reaches $\Gamma_{\rm min}$. Considering $x^i = \theta$ in Equation (10) and for the jet Lorentz factor profile given by Equation (16), the sign for $\frac{\partial \log \Gamma}{\partial \theta}$ is negative but the whole term

[2] This is a valid approximation, as $r_0 \ll r_{\rm ph}$.

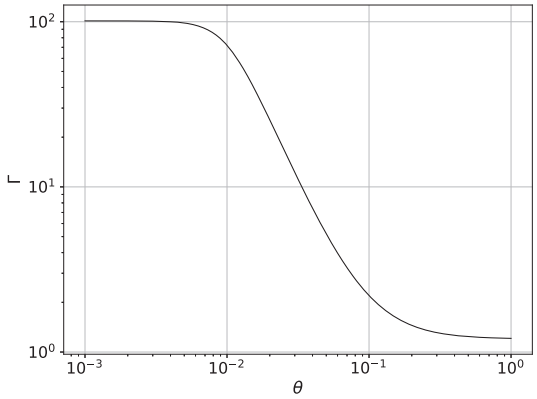

Figure 2. Lorentz factor (Γ) profile of the jet characterized by Equation (16) with parameters $p = 2.0$, $\theta_j = 0.01$ rad, $\Gamma_0 = 100$, and $\Gamma_{min} = 1.2$. $\theta_e = \theta_j \Gamma_0^{1/p}$. The inner jet region is for $\theta < \theta_j$ while outer region extends beyond θ_e. The region bounded within $\theta_j - \theta_e$ harbors an effective velocity shear leading to photon energy gain.

$\frac{\partial \log \Gamma}{\partial \theta} \delta\theta$ is positive for negative $\delta\theta$, which implies scattering toward the inner region of the jet or toward the jet axis. It means that the photon gains energy when it is scattered inward ($g > 1$) while it loses energy when it scatters away ($g < 1$). The scattering takes place with the condition $\Gamma_{min} < \Gamma_2 < \Gamma_0$ in Equation (9). For such a jet, the comoving electron number density is $n_e' = L/4\pi m_p c^3 v \Gamma^2 r^2$, where L is the angle independent[3] jet luminosity and v is the bulk jet speed in units of c. One therefore concludes that $a = vr/2r_{ph}$ and the photospheric radius for an on-axis observer r_{ph}(observer's angle $\theta_o = 0$) is given by $r_{ph} = \sigma L/8\pi c^3 m_p \Gamma^3$ (see Lundman et al. 2013 for further details). The optical depth for photon propagation along the radial direction is a strong function of the propagation angle, θ. In the inner jet region ($\theta < \theta_j$), the optical depth along the photon's path is significantly smaller than the outer region (as $\tau_1 \propto 1/\Gamma^3$). Thus, the photons easily escape the jet once they reach the inner region. Hence, the angular limit $\theta_b = \theta_j$ is an effective boundary for photon escape for the case of a GRB jet. As the photons escape to the inner region of the jet before leaving the system, the on-axis observer is likely to observe a brighter spectra compared to the off axis observers.

Assuming a constant Lorentz factor Γ along the photon's path, it can be taken outside the integration in Equation (13). This assumption means that while calculating the mean free path at a certain location along a small angle $1/\Gamma$, one can approximate that the Lorentz factor of the outflow encountered by the photon is $\approx\Gamma$. It enables an analytical estimate of τ_2 and is justified because the photon escapes to the inner region ($\theta < \theta_j$) only when it is very close to the boundary ($\theta \sim \theta_j$) where the Lorentz factor does not vary much along the photon's path (Figure 2). Noting that $1 - v\cos\theta_s \approx 1/\Gamma^2$, the optical depth can be written as

$$\tau_2 = \frac{2r_{ph}}{v} \int_0^{s_0} \frac{ds}{r'(s)^2}. \tag{17}$$

Here $r'(s) = r + s\cos\theta_s$ is the radial coordinate along path s. Direct integration gives

$$\tau_2 = \frac{2r_{ph}}{vr\cos\theta_s} \left[1 - \frac{1}{(\theta - \theta_j)\Gamma\cos\theta_s + 1} \right]. \tag{18}$$

We use Equations (16)–(18) and follow the procedure described above to calculate the observed photon index β (Equation (15)) produced by a GRB jet. The integration over the jetted region $\theta_j - \theta_e$ and $r_0 - r_{ph}$ is performed as there is no significant photon energy gain in the regions $\theta < \theta_j$ and $\theta > \theta_e$.

4. Results and Discussion

We consider $\Gamma_0 = 100$, $\theta_j = 0.01$ rad, $d = 20$, and $\varepsilon_0 = 10^{-6} \times$ rest mass energy of electron. The observer is situated at the jet axis; $\Gamma_{min} = 1.2$ and $L = 10^{52}$ ergs. The simulated spectra for $p = 2.5$, 4.0, and 6.0 are plotted with a black solid curve in the first three panels of Figure 3. The best fit to the high energy tail is shown by blue dotted lines. We emphasize that the simulation code is based upon the Monte Carlo technique, where we track every photon that scatters within the jet until it escapes. Then the final count of the photons within a given observer angle is distributed along with the escaped energies. (see Pe'er 2008, Lundman et al. 2013, and Vyas et al. 2021a for the code structure and respective details). In the last panel of Figure 3, we compare the photon indices associated with the power-law spectra at high energy obtained by simulations (dots) with ones calculated analytically (dashed curve) using Equation (15). The simulated photon indices are in agreement with the calculated slopes. For the reasons given above, photons' energy loss due to expansion dominates over energy gain by velocity shear for small values of profile index ($p < 2$) and there is no high energy power laws below this threshold. From the simulations, we map the density distribution of photons' angular location (θ_{escape}) at the moment of escape with the escape energy in Figure 4. The parameters are kept the same with top left panel of Figure 3. The horizontal red line separates photons that form a high energy tail to the photons that form the low energy portion of the spectrum. In accordance with our expectations, most of the photons that take part in producing the high energy spectrum escape from the inner region of the jet. The photons that escape at larger angles, take part in the low energy portion of the spectrum. The low energy part of these spectra was theoretically modeled by Lundman et al. (2013) while we have modeled the high energy power law in this Letter. An additional feature predicted by this figure is that the inner funnel of the jet is virtually empty due to very low optical depths. Hence the visual appearance of the jet should have more photons from the immediate outer angular regions at large distances.

In the upper two panels of Figure 5, we include the simulated spectra for $\Gamma_0 = 300$ with $p = 2.5$ and 6.0, keeping other parameters same as Figure 3. In the bottom panel of this figure, we plot the analytic curves of β as a function of p for $\Gamma_0 = 100$ (solid blue curve) and 300 (dashed black curve). The simulated spectral slopes are shown by blue stars and black filled circles respectively. The theoretical values are able to predict the

[3] The assumption that L is angle independent is justified in the case of GRBs due to narrow jets. The prominent portion of the observed spectrum in the GRB prompt phase consists of photons that make their last scattering within an angle below $5/\Gamma_0$. As shown in Zhang et al. (2003), at the largest radii of their simulations, $\Gamma_0 \sim 140$ by $\theta \sim 0.02$ rad, while the luminosity is seen to be constant up to 0.05 rad (or $7/\Gamma_0$) (see the top panels of their Figures 8 and 9). Hence for theoretical considerations, $L(\theta) =$ constant is a reasonable assumption (also see the relevant discussions in Lundman et al. 2013).

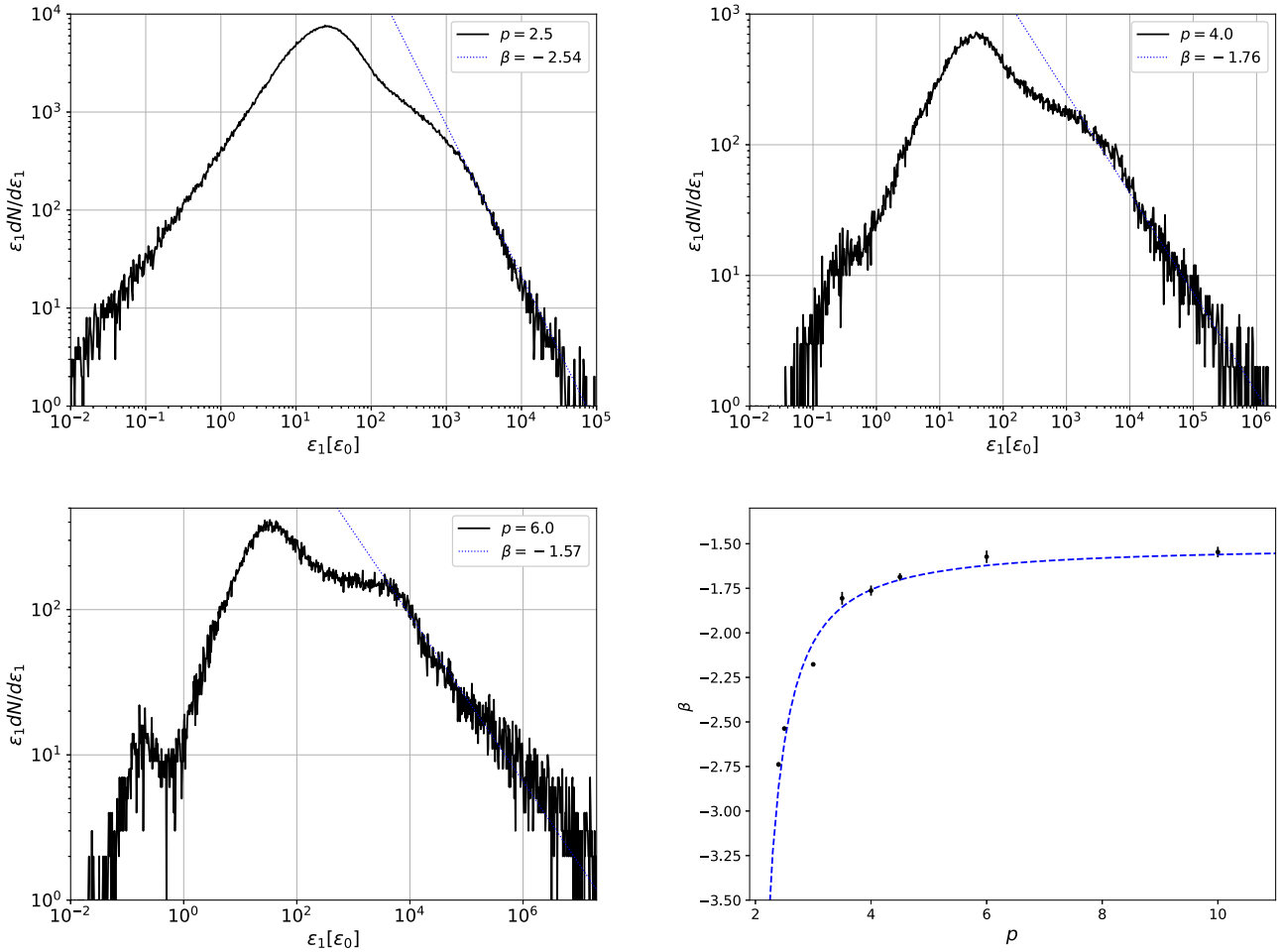

Figure 3. Spectra obtained by numerical simulations for $\Gamma = 100$, $p = 2.5 - 6$ (solid black) along with fits (dotted blue) for high energy slopes β. The low energy part of these simulated spectra was modeled by Lundman et al. (2013) and we explain the high energy power-law spectrum. The last panel shows the variation of analytically calculated β as a function of p (blue dashed). The simulated photon indices are overplotted by black solid points and are found to be in good agreement with the theoretical curve. The slopes are fitted with power-law indices in the high energy range and the respective error bars in simulated points for β are the associated standard deviation. Here $\theta_j = 0.01$ rad, $\Gamma_{min} = 1.2$, and $L = 10^{52}$ erg s^{-1}, the monoenergetic seed photons are injected with energy $\varepsilon_0 = 10^{-6}$ (in the units of the rest mass energy of the electron) in the Monte Carlo Simulation code with identical parameters at radial coordinate $r_0 = r_{ph}/d$. Depth $d = 20$ ensures that the photons are injected deep inside the flow. The spectra are seen by an on-axis observer at $\theta_o = 0$ rad (i.e.,the populations of photons escaped within an angular bin $\theta = 0$–0.02 rad). The total number of photons injected is 4 million, 2 million, and 2.6 million for $p = 2.5$, 4.0, and 6.0, respectively.

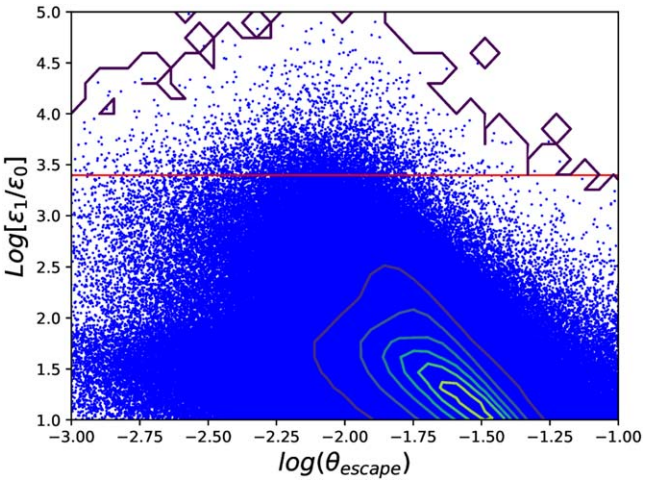

Figure 4. Density distribution of individual photons over the angular location at the time of escape for $p = 2.5$, $\theta_j = 0.01$ rad, and $\Gamma_0 = 100$. The distribution marks that most photons that form a high energy tail (above $\varepsilon_1/\varepsilon_0 \sim 2.5 \times 10^3$) escape from the inner region of the jet below θ_j. The photons escaped from larger angles ($\theta > \theta_j$) mostly contribute to the low energy potion of the emitted spectrum.

differences in the values of β with p as well as with Γ_0 confirming the model.

Due to the complexity of the integrals in Equations (11) and (12), exact analytic expression of the photon indices in the general case is not possible to obtain. However, one can obtain an analytic expression for the asymptotic behavior of β as $p \to \infty$ as follows. Assuming $\tau_2 \ll 1$ or $P(r, \theta) \sim \tau_2$ analytic integration gives $\bar{g} \propto p^2$ and $\bar{P} \propto (\Gamma_0^{1/p} - 1)$, which lead to $\beta \to -1.5$. This is indeed seen in Figure 3 for both the semianalytic results as well as in the simulated slopes.

Quantitatively, tackling the case of a GRB jet with a structured Γ profile as a function of polar angle θ, the Comptonized photons can extend up to several orders of magnitude. The produced power-law spectrum at high energies is capable of explaining the high energy tails generally observed in the GRB prompt phase. We analyzed that the photon indices of these spectra largely depend upon p, which determines the sharpness of the decay of Γ with θ. The photon index β ranges from $-\infty$ to -1.5. This is indeed seen in Figures 3 and 5 for both the semianalytic and the simulated results of β. It is worth mentioning that β in the GRB prompt

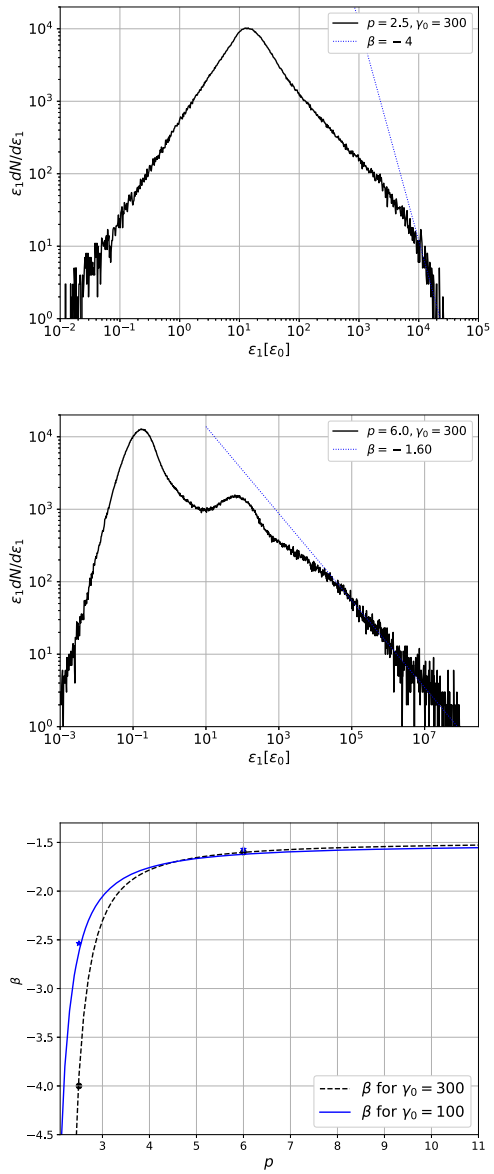

Figure 5. Top panel: simulated spectrum for $\Gamma_0 = 300$ and $\theta_j = 0.01$ rad and $p = 2.5$ (black solid curve). Other parameters are the same as Figure 3. Middle panel: same as the top panel but for $p = 6.0$. In both the panels, the blue dotted line is the best fit to the spectra at high energy producing simulated β. In the bottom panel, we plot the theoretical values of β as a function of p for $\Gamma_0 = 100$ and 300 with blue solid and black dashed curves respectively and overplot the simulated values of β by blue star ($\Gamma_0 = 100$) and black filled solid ($\Gamma_0 = 300$).

phase observations are found to be between -4 and -1.5 (Preece et al. 2000; Kaneko et al. 2006; Pe'er 2015) and this range is in agreement with our results. Inversely, using the observed values of β, we can directly constrain the jet structure of these bursts.

Although the physical picture of the photon energy gain described here has similarities with the second-order Fermi acceleration of massive particles, important differences must be highlighted. In analytical calculations of the Fermi acceleration process, the expectation value of the gain and the scattering probability are averaged over scattering angles. In the currently discussed mechanism, the energy gain not only depends upon the scattering angle but also on the scattering location. Hence, one needs to average the gain and the scattering probability over the entire scattering region to obtain their expected values. Furthermore, the escape of photons from the inner jet boundary adds an extra constraint on the escape probability as the jet Lorentz factor profile leads to local anisotropy in the flow.

5. Conclusions

We conclude that the commonly observed high energy power-law spectra from various astrophysical sources can have a natural origin due to repeated scattering of photons in relativistic flows with velocity shear. Thus, we provide a novel and viable alternative to the generally considered processes such as synchrotron and inverse thermal Comptonization. These mechanisms need the presence of highly relativistic electrons while in current work the bulk kinetic energy of the jet is transferred to the photons leading to a high energy tail excluding the presence of high energy particles as a prior requirement.

Our analytic approach involves the averaging of photon energy gain over volume of the accelerating region between $\theta_j - \theta_e$. The theoretical estimates explain the generation of power-law spectra and also capture microscopic quantitative features of the spectra at high energies, such as (i) the variation of spectral slopes with the dynamic parameters is identical between numerical as well as analytical calculations and the similarity is very accurate, (ii) vanishing of power-law spectra (the cut off in the $\beta - p$ plot, last panel of Figure 3) for small and nonzero values of p as it appears due to the radial expansion of the jet, and (iii) asymptotic saturation of spectral slopes β reach as $p \to \infty$.

As we restrict the framework up to relativistic jets in this work, in future we will extend it to mildly relativistic systems as well as nonrelativistic plasma with velocity shear.

A.P. acknowledges support from the European Union (EU) via ERC consolidator grant 773062 (O.M.J.). M.K.V. acknowledges the PBC Fellowship by the government of Israel as well as part of funding obtained by the abovementioned ERC grant.

ORCID iDs

Mukesh K. Vyas https://orcid.org/0000-0001-6560-0902
Asaf Pe'er https://orcid.org/0000-0001-8667-0889

References

Aneesha, U., & Mandal, S. 2020, A&A, 637, A47
Band, D., Matteson, J., Ford, L., et al. 1993, ApJ, 413, 281
Barraud, C., Olive, J. F., Lestrade, J. P., et al. 2003, A&A, 400, 1021
Blandford, R., & Eichler, D. 1987, PhR, 154, 1
Bošnjak, Ž., Götz, D., Bouchet, L., Schanne, S., & Cordier, B. 2014, A&A, 561, A25
Burgess, J. M., Preece, R. D., Connaughton, V., et al. 2014, ApJ, 784, 17
Cohen, E., Katz, J. I., Piran, T., et al. 1997, ApJ, 488, 330
Doeleman, S. S., Fish, V. L., Schenck, D. E., et al. 2012, Sci, 338, 355
Frontera, F., Amati, L., Costa, E., et al. 2000, ApJS, 127, 59
Fukue, J. 2021, MNRAS, 503, 1367
Ito, H., Nagataki, S., Ono, M., et al. 2013, ApJ, 777, 62
Junor, W., Biretta, J. A., & Livio, M. 1999, Natur, 401, 891
Kaneko, Y., Preece, R. D., Briggs, M. S., et al. 2006, ApJS, 166, 298
Kaufman, J., & Blaes, O. M. 2016, MNRAS, 459, 1790
Kaufman, J., Blaes, O. M., & Hirose, S. 2017, MNRAS, 467, 1734
Kylafis, N. D., Reig, P., & Spruit, H. C. 2003, in ASP Conf. Ser. 308, From X-ray Binaries to Gamma-Ray Bursts: Jan van Paradijs Memorial Symposium, ed. E. P. van den Heuvel et al. (San Francisco, CA: ASP), 153
Le, T., Newman, W., & Edge, B. 2018, MNRAS, 477, 1803
Levinson, A., & Eichler, D. 1993, ApJ, 418, 386
Lundman, C., Pe'er, A., & Ryde, F. 2013, MNRAS, 428, 2430
MacFadyen, A. I., & Woosley, S. E. 1999, ApJ, 524, 262

Nandra, K., & Pounds, K. A. 1994, MNRAS, 268, 405
Page, K. L., Reeves, J. N., O'Brien, P. T., & Turner, M. J. L. 2005, MNRAS, 364, 195
Pe'er, A. 2008, ApJ, 682, 463
Pe'er, A. 2015, AdAst, 2015, 907321
Pe'er, A., & Ryde, F. 2017, IJMPD, 26, 1730018
Preece, R. D., Briggs, M. S., Mallozzi, R. S., et al. 2000, ApJS, 126, 19
Preece, R. D., Pendleton, G. N., Briggs, M. S., et al. 1998, ApJ, 496, 849
Reeves, J. N., & Turner, M. J. L. 2000, MNRAS, 316, 234
Reig, P., Kylafis, N. D., & Spruit, H. C. 2001, A&A, 375, 155
Ryde, F., & Pe'er, A. 2009, ApJ, 702, 1211
Schaefer, B. E., Palmer, D., Dingus, B. L., et al. 1998, ApJ, 492, 696
Tavani, M. 1996, ApJ, 466, 768
Vyas, M. K. 2022, Univ, 8, 294
Vyas, M. K., & Chattopadhyay, I. 2017, MNRAS, 469, 3270
Vyas, M. K., & Chattopadhyay, I. 2018a, A&A, 614, A51
Vyas, M. K., & Chattopadhyay, I. 2018b, JApA, 39, 12
Vyas, M. K., & Chattopadhyay, I. 2019, MNRAS, 482, 4203
Vyas, M. K., Kumar, R., Mandal, S., & Chattopadhyay, I. 2015, MNRAS, 453, 2992
Vyas, M. K., Pe'er, A., & Eichler, D. 2021a, ApJ, 908, 9
Vyas, M. K., Pe'er, A., & Eichler, D. 2021b, ApJL, 918, L12
Wang, X.-Y., Li, Z., Dai, Z.-G., & Meszaros, P. 2009, ApJL, 698, L98
Woosley, S. E. 1993, AAS Meeting, 182, 55.05
Yu, H.-F., Greiner, J., van Eerten, H., et al. 2015, A&A, 573, A81
Zdziarski, A. A., Malyshev, D., Chernyakova, M., & Pooley, G. G. 2017, MNRAS, 471, 3657
Zhang, W., Woosley, S. E., & MacFadyen, A. I. 2003, ApJ, 586, 356